THE NOBEYAMA RADIOHELIOGRAPH — HARDWARE SYSTEM —

M. Nishio [1], H. Nakajima [1], S. Enome [1], K. Shibasaki [1], T. Takano[1], Y. Hanaoka [1], C. Torii [1], Y. Shiomi [1], H. Sekiguchi [1], T. Bushimata [1], S. Kawashima [1], N. Shinohara [1], H. Koshiishi [1,2], T. Kosugi [1], M. Sawa [1], K. Kai [1*], Y. Irimajiri [3], H. Nohmi [4], K. Honda [4], H. Shinohara [4], T. Ito [4], M. Miyawaki [4], A. Imoto [5], T. Takabayashi [6], K. Nishikawa [7], N. Futagawa [7], S. Tanaka [8], H. Morikawa [9], Y. Kitahara [9], K. Harakawa [10], and K. Mishima [11]

[1] *Nobeyama Radio Observatory, National Astronomical Observatory, Minamisaku, Nagano 384-13, Japan*
[2] *Department of Astronomy, School of Science The University of Tokyo, Bunkyo-ku, Tokyo 113, Japan*
[3] *Communications Research Laboratory, Koganei, Tokyo 184*
[4] *Guidance and Electro-optics Division, NEC Corporation, Nisshin-cho 1-10, Fuchu, Tokyo 183, Japan*
[5] *2nd Government System Division, NEC Corporation, Shiba 12-7-17, Minato-ku, Tokyo 105, Japan*
[6] *Space System Division, NEC Corporation, Ikebe 4035, Midori-ku, Yokohama 226, Japan*
[7] *Space System Development Division, NEC Corporation, Ikebe 4035, Midori-ku, Yokohama 226, Japan*
[8] *Sumitomo Electric Industries Ltd. Yokohama Laboratory, Taya 1, Sakae-ku, Yokohama 224, Japan*
[9] *Akasaka Diesels Ltd., Nakaminato 4-3-1, Yaizu, Shizuoka 425, Japan*
[10] *Hodensha Co. Ltd., Echigoshima 357, Yaizu, Shizuoka, Japan*
[11] *Pasco Corporation, Higashiyama 2-13-5, Meguro-ku, Tokyo 153, Japan*

Abstract

The Nobeyama Radioheliograph began routine observations in late June, 1992, and radio full-disk images of the Sun have been observed for 8 h every day. This instrument is a 17-GHz radio interferometer dedicated for solar observations, which consists of eighty-four

* Deseased

80-cm-diameter antennas arranged in a Tee-shaped array extending 490 m in east-west and 220 m in north-south directions. The spatial resolution is 10″ and the temporal resolution is 1 s and 50 ms for selected events. The array configuration is optimized to observe the whole sun with high spatial and temporal resolution and a high dynamic range of images. Image quality of better than 20 dB is realized by incorporation of technical advances in hardware and software, such as (1) low-loss phase-stable optical fiber cables for local reference signal and IF signals, (2) newly developed phase-stable local oscillators, (3) custom CMOS gate-array LSIs of one-bit quadra-phase correlators for 4×4 combinations, (4) an expanded real-time self-calibration method of gain and phase errors using redundant antenna combinations, and (5) new image processing techniques to suppress large sidelobe effects due to the solar disk and extended sources. A newly developed control system with fully distributed computers enable us to continue observations even in a condition where some portions of the radioheliograph are malfunctioning. In this paper, a detailed description is given of the radioheliograph's hardware, with particular emphasis on the stability and accuracy of the total system.

1. Introduction

Radio imaging observations have an important role to reveal the physical mechanism of solar flares. They will give us new information about locations of electron acceleration sites. In addition, as the radio emission is quite sensitive to magnetic field configurations of emitting region, we can obtain information about the coronal magnetic field. Usually, the flaring regions have complicated geometrical configurations. Therefore, two-dimensional imaging observations are quite essential. Clearly, high spatial resolution is required to resolve radio sources on the Sun. Solar flares typically show impulsive time variations at their early phase and quick changes of geometrical configurations can be expected. Therefore, a high temporal resolution is required of observation instruments.

High-resolution imaging observations of the Sun have been carried out in microwaves using large interferometers such as the Very Large Array (Napier et al. 1983) and the Westerbork Synthesis Radio Telescope (Baars et al. 1973), which are mainly designed for rotational synthesis observations and suitable to observe quasi-stationary objects such as cosmic radio sources or solar active regions. These instruments consist of element antennas of large diameter designed for their large collecting area which gives a narrower field of view. In this type of instrument, the observation time is shared with various solar and non-solar projects according to observation proposals. In solar flare studies, statistical or systematic observations are quite essential to reveal general properties of the flare, and a dedicated instrument is required to routine base observations with a wide field of view to cover the whole Sun.

The Nobeyama Radioheliograph began routine observations in late June 1992, which was constructed in two years of fiscal years 1990 and 1991. This instrument is a radio interferometer dedicated to solar observations and has excellent performance of high spatial and temporal resolution imaging of the whole Sun with high image quality. From the start of routine observations, many interesting phenomena concerning with solar flares, prominence eruptions and S-components have been observed, and several remarkable results have been reported (Enome et al. 1993; Enome et al. 1994; Hanaoka et al., 1994a; Nishio et at. 1994; Shibasaki et al. 1994a; Shibasaki et al. 1994b; Takano et al., 1994a; Takakura et al. 1994).

Overall description of the radioheliograph was previously given by Nakajima et al. (1984). In this paper, we describe the hardware system in detail. Description of data storage and processing system is given in another paper in this proceedings (Hanaoka et al. 1994b). In section 2, major characteristics of the radioheliograph are given. In section 3, 4, 5, and 6, an antenna system, a receiver system, a signal transmission system and a control system of the radioheliograph are described, respectively, with particular emphasis on the stability and accuracy of the total system. In section 7, the total performance of the radioheliograph hardware is discussed.

Table 1. Nobeyama Radioheliograph characteristics and performance

Observing Frequency	17 GHz (λ = 1.7635 cm)
Bandwidth	33.6 $\pm$ 1.7 MHz (Asymmetry among antennas: < 0.6 dB)
Field of View	40′
Spatial Resolution	10″ for 2-d images 5″ for east-west 1-d images
Temporal Resolution	1 s for entire obs. period, 50 ms for selected events
Dynamic Range of Images	$\geq$ 20 dB for snapshot $\geq$ 30 dB for rotational synthesis
Observing period	$\pm$ 4 h around meridian time of about 0245 UT
Sensitivity in Solar Obs. Flux Density (Brightness Temp.)	4.4×10^{-3} sfu (1300 K)*1 for 1 s snap shot 7.3×15^{-5} sfu (22 K) for 1 h rotational synthesis
Polarization	Both circular polarization (time sharing every 25 ms)
Isolation of Polarization SW	$\geq$ 20 dB (several: 18 dB)
Overall Phase Stability	$\leq$ 0.3 (rms)
Overall Gain Stability	$\leq$ 0.2 dB (rms)

*1 1 sfu = 10^{-22} W m^{-2} Hz^{-1}.

2. Major Characteristics

In solar flare observations, the observation frequency should be in short- centimeter to millimeter wavelengths where radio sources are optically thin, and preferably multi-frequency in order to determine frequency spectra and hence energy distribution of accelerated electrons. In the radioheliograph, the observation frequency is chosen to be 17 GHz as an initial step, and an expansion plan is considered of simultaneous operations at 17 GHz and 34 GHz in the near future (Takano et al. 1994b). At 17GHz, the radio emission from electrons accelerated up to about 100 keV is dominant in impulsive phase of flares, and has close correlation with the hard X-ray emission.

The spatial resolution of the radioheliograph is given by the ratio of observation wavelength and maximum antenna spacing projected on a plane normal to the direction of the Sun. Therefore, the spatial resolution varies by the direction of the Sun. The nominal spatial resolution is about 10″ for two dimensional images and 5″ for east-west one dimensional images, which are given when the Sun is at the zenith direction and at the meridian of the radioheliograph, respectively. The field of view of the radioheliograph is given by the ratio of observation wavelength and projected fundamental antenna spacing, and is also a function of the direction of the Sun. The nominal field of view is 40′, and is wide enough to cover the whole Sun.

The dynamic range of images is better than or equal to 20 dB for snap-shots. At early phase of flares, thermal radio emission is usually weaker than the nonthermal radio emission and vice versa at late phase of flares. The high dynamic range of the radioheliograph enables us to observe the thermal and the nonthermal phenomena simultaneously. Therefore, detailed analysis is possible about relations between both phenomena. In the radioheliograph, absolute

source positions are determined by using the solar limb as a reference. Therefore, it is quite essential to observe the flaring region and the solar disk simultaneously. For usual flares, the dynamic range of the radioheliograph is sufficient to determine the absolute source position.

The temporal resolution of the radioheliograph is 1 s for entire observation period of 8 h, and 50 ms for selected events. This maximum temporal resolution of 50 ms is determined to trace streaming of energetic electrons from particle acceleration sites with 10″ spatial resolution.

Circular polarization measurements are important in solar radio observations to reveal relations between the coronal magnetic field and energetic electrons. In the radioheliograph, a polarization degree of about 1 % is detectable. Each polarization data is measured by time sharing every 25 ms.

The major characteristics of the radioheliograph are shown in Table 1.

Table 2. Parameters of the Antenna Array

Total Baseline Length	488.960 m for EW array 220.060 m for NS array*1
Fundamental Spacing (d)	1.528 m
Antenna Spacing	(1, 2, 4, 8, 16) × d
Location of Array Center	Longitude 138° 28′ 37.″14 Latitude 35° 56′ 20.″04
Number of Antennas	84
Diameter of Element Antenna	80 cm
Half-Power Beamwidth of Element Antenna	87.′1 ± 0.′4 at 17 GHz
Antenna Temperature (Sun)	550 K (average) at 17 GHz
Overall Pointing Error	< 1.′5

*1 EW base line is on the horizontal line, while NS base line inclines by 1.4998/100 toward the north.

3. Antenna and Array Configuration

The antenna array of the radioheliograph is arranged to be suitable for imaging of rapidly changing phenomena. The array has a multiple, equally spaced Tee-shaped configuration, which extends 488.960 m in the east-west direction and 220.060 m in the north-south direction. Eighty-four antennas with 80-cm diameter are placed with increasing antenna spacing such as d (fundamental spacing), 2d, 4d, 8d and 16d from the phase center of the Tee-array. The central portion with short antenna spacing is used to synthesize high-quality images of the whole Sun, which are used to calibrate the location of the solar disk. The outline of the array is shown in photo 1 and the geometry of antenna allocation is given in figure 1.

The antennas of the radioheliograph have a Cassegrain-type antenna optics with main reflectors of 80-cm diameter. An appearance of the element antenna is shown in photo 2. The half-power beamwidth of the reflector is 87.′1 ± 0.′4, which results to a degradation of the gain by 9 % at the solar limb, if the antenna points to the center of the Sun. Pointing errors of the element antennas result in correlator-based phase and amplitude errors of observed spatial Fourier components, which cannot be corrected after observations. The pointing errors are, therefore, serious to an extended source such as the quiet Sun. Mechanical pointing accuracy of less than 30″ is obtained for all antennas and this is sufficient value. Each antenna is supported by an alt-azimuth mount, which was chosen because it is easy to be set in the required position with a specified accuracy, as compared with the equatorial mount.

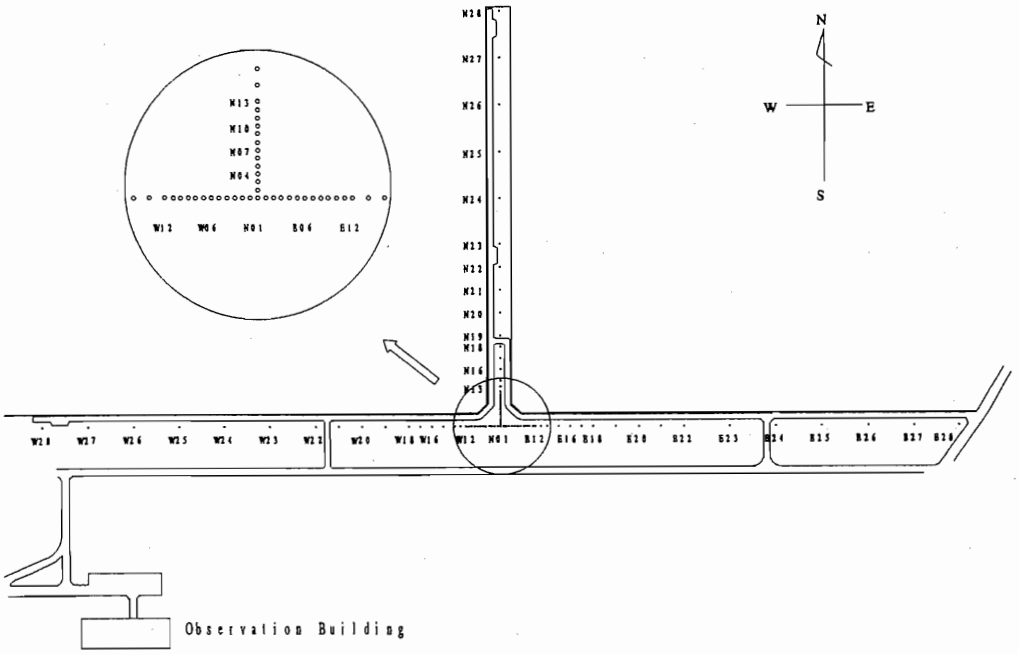

Fig. 1. Geometrical layout of the antenna array of the Nobeyama Radioheliograph.

The antennas are placed at the designed horizontal and vertical positions within the accuracy of 0.5 mm rms. The antenna positions are adjusted with 18 first order control points as reference points, which are fixed precisely by a method using geodetic network (Mishima et al. 1992). This accuracy is necessary to keep the phase errors due to the setting errors of antennas as small as 3° or less for 1-h aperture synthesis observations. In order to keep this position accuracy in the ambient temperature variation from −30 °C to 30 °, each antenna is placed on a pile of 5 m length and 0.35 m diameter, which is buried under the ground.

4. Receiver System

The receiver system of the radioheliograph consists of front-end receivers placed at each antenna site, and an IF receiver and a digital back-end receiver installed in the observation building. A block diagram of the receiver system is shown for only a receiver channel in figure 2. Each front-end receiver is installed in a front-end box, which is fixed to a backside of the main reflector of antenna optics. At the front-end receiver, the signals received at each antenna are amplified, and then down-converted to IF signals at 200 MHz. The front-end receivers and the IF receiver are connected with phase-stable optical fibers where the IF signals and a reference signal of local oscillators are transmitted. At the digital back-end receiver, the received signals are cross-correlated to obtain spatial Fourier components of solar radio images. The correlation data are transmitted to a host computer through an Ethernet line, and are recorded onto optical disks in real time. Recorded data are not solar radio images, but are correlation data because of limits of computing power for real-time image processing. The image synthesis is performed by off-line processing. Usually correlation data with 1-s time resolution are recorded for 8 h in a day. In addition, correlation data with 50-ms time resolution are recorded for selected events with short duration such as impulsive phase of bursts.

In the radioheliograph, precise measurements of phase relations among the received

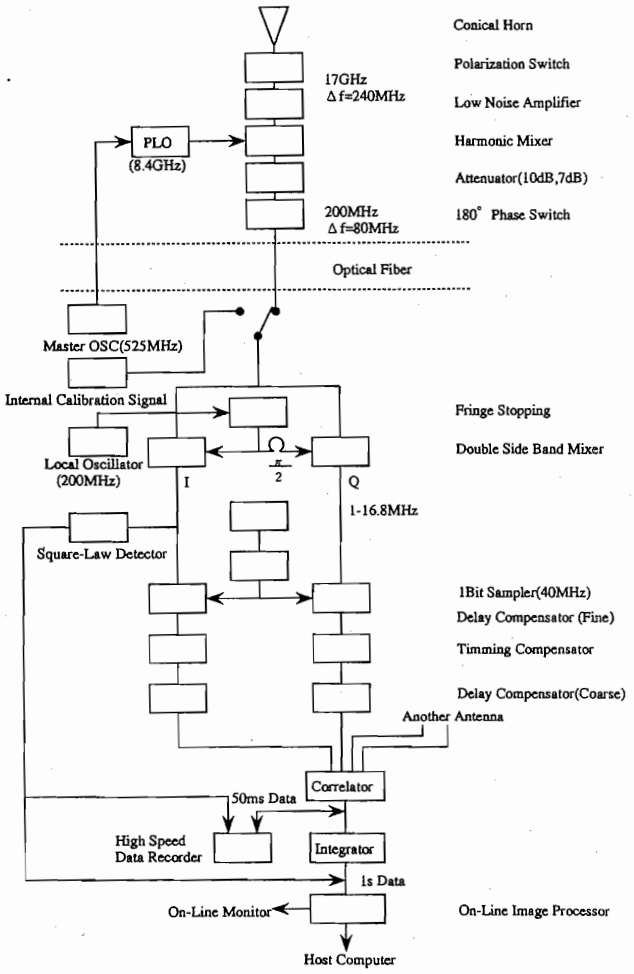

Fig. 2. Block diagram of the receiving system.

signals are quite essential to synthesize high quality images. In order to obtain good phase stability of the receivers, distributions of a phase- stable local oscillator signal (LO signal) to the antennas is a key issue. The LO signal at 8.4 GHz, which is used to the frequency down-conversion at the front-end receiver, is phase-locked to the reference signal of 525 MHz, which is sent to each antenna through a 1-to-84 optical divider and phase-stable optical fiber cables from the master oscillator in the observation building.

4.1. Front-end Receiver

In the radioheliograph, the right- and left-handed circular polarization signals are received alternatively every 25 ms through polarization switches mounted to each antenna. Isolation of better than 20 dB is obtained between right- and left-handed circular polarizations for most antennas.

The RF signals of 17 GHz are amplified by an uncooled HEMT amplifier with an average noise temperature of 180 K, which is installed close behind the polarization switch within each front-end box. The overall receiver noise temperature is 360 K, which includes the insertion loss of the feed-horn and the polarization switch. An output frequency of the local oscillator is 8.4 GHz, and the frequency down-conversion is performed by a harmonic mixer.

The IF signal is modulated, making use of the Walsh function with 180 ° phase switch inserted in the IF line and demodulated after analog-to-digital conversion of the digital back-end. This phase switching mechanism reduces the cross-talk among the IF signals and external interference to the IF signal by about −30 dB.

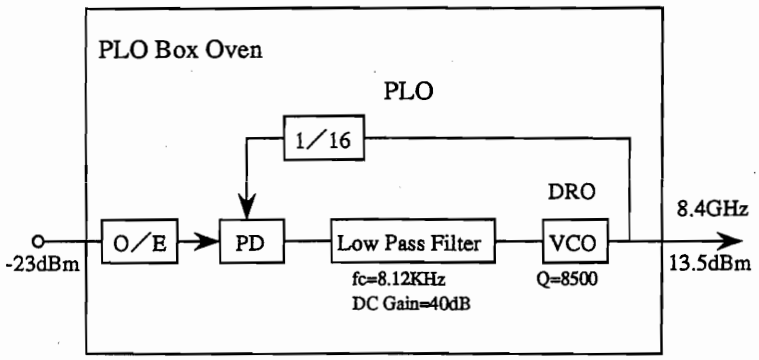

Fig. 3. Block diagram of the phase-locked oscillator.

Phase lock of the local oscillator is achieved by comparing the phase between the reference signal of 525 MHz and the down-converted signals of local oscillator output obtained by using a digital frequency divider. Figure 5 is a block diagram of the phase-locked oscillator installed in the front-end receiver. As the phase-lock circuit has a rather high temperature coefficient (8. °5 / °C at 8.4 GHz), it is enclosed in a small box in which the temperature is maintained within 40 ± 0.1 °C using a Peltier cooling unit. As the optical-to-electrical converter (O/E converter) has also high temperature coefficient of −5 ° /°C at 8.4 GHz, it is enclosed in the same box. As a result, the overall temperature coefficient of the phase-locked oscillator is −1. °3/°C, which includes the O/E converter.

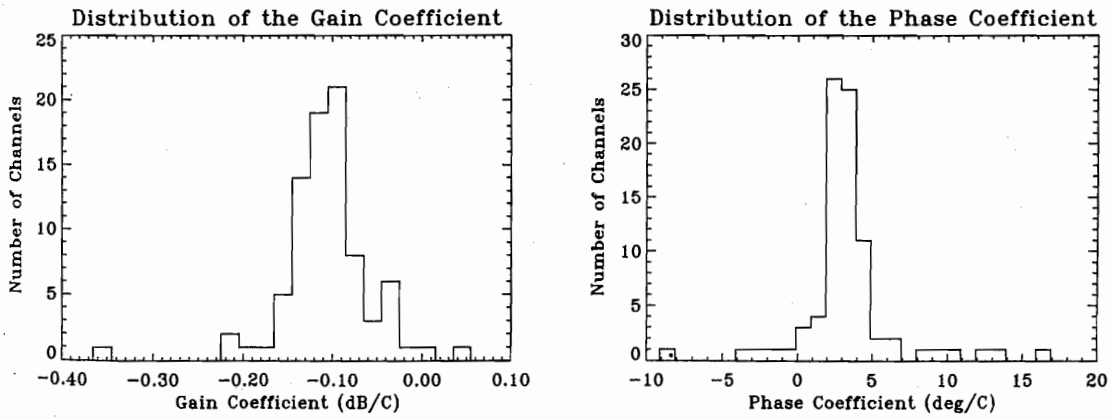

Fig. 4. Overall temperature coefficient of gain and phase of the front-end receivers.

The gain and the phase of the front-end receiver are quite sensitive to ambient temperature variations. The overall temperature coefficient of gain and phase of the front-end receivers are shown in figure 6. Gain and phase variations of the front-end receiver are about

-0.1 dB / °C and 0.°3 / °C respectively for almost all antennas, where the phase variations are counted at 17 GHz. In order to reduce the affection of ambient temperature variations, the temperature of the front-end box is controlled within 35 ± 1 °C.

4.2. IF Receiver

At the IF receiver, the IF signal transmitted from each antenna is converted to two baseband signals orthogonal to each other by double sideband mixers. The baseband signals have a frequency range from 100 kHz to 16.8 MHz. Phase angles between mutually orthogonal signals are adjusted to be 90° ± 0.°6 for all receiver channels. In order to stop the fringe variations, the phase rotator is inserted on the local signal line. The phase is changed in steps of 0.°36 with the overall accuracy better than ±0.°6.

4.3. Digital Back-end Receiver

In the radioheliograph, complex correlations are calculated for all antenna pairs of 3486 combinations of 84 antennas. This calculation is made by one-bit correlators (Weinreb 1963), which can be assembled with simple digital logic circuits, and yields great stability to the back-end. In the case of solar observations, the received signal is so strong that the loss of sensitivities by a factor of $2/\pi$ is not severe.

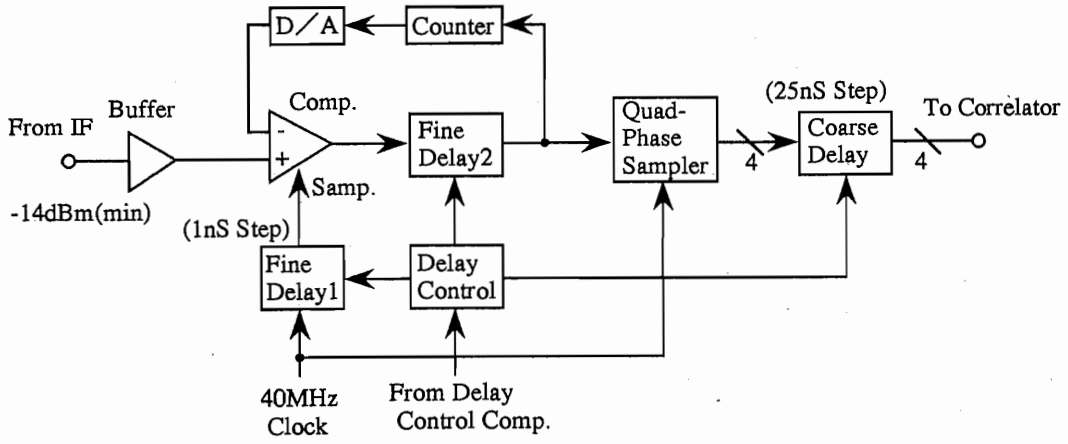

Fig. 5. Block diagram of the A/D converter.

Figure 7 shows an analog-to-digital converter (A/D converter) of the radioheliograph, where the received signal converted to the baseband range is digitized to one-bit data by a sampling clock at 40 MHz. Differences of signal arrival time among antennas are digitally compensated by a step of 1 ns with accuracy of less than 1 ns. This compensation is performed by combining a fine delay with the range from 0 ns to 24 ns and a minimum step of 1 ns and a coarse delay with the range from 0 ns to 1700 ns and a unit step of 25 ns. The former is performed by shifting the sampling clock and the latter is performed by using a shift-register attached to the output of a one-bit sampler. As large offsets of the one-bit samplers result in correlation errors, the offsets are compensated by counting the difference of 0 state and 1 state of the sampler output during about 50 ms and then returning it to the sampler input through a digital-to-analog converter (D/A converter). The offset voltage at the sampler input is suppressed to be less than 0.5 mV for the input signal range from 60 mV to 320 mV.

For the correlator system, a specially designed correlator chip was developed using a CMOS gate array with 30,000 gates (Nishio et al. 1992a). This chip is composed of 16 complex correlator units, which corresponds to 4 × 4 combinations of antennas, and each

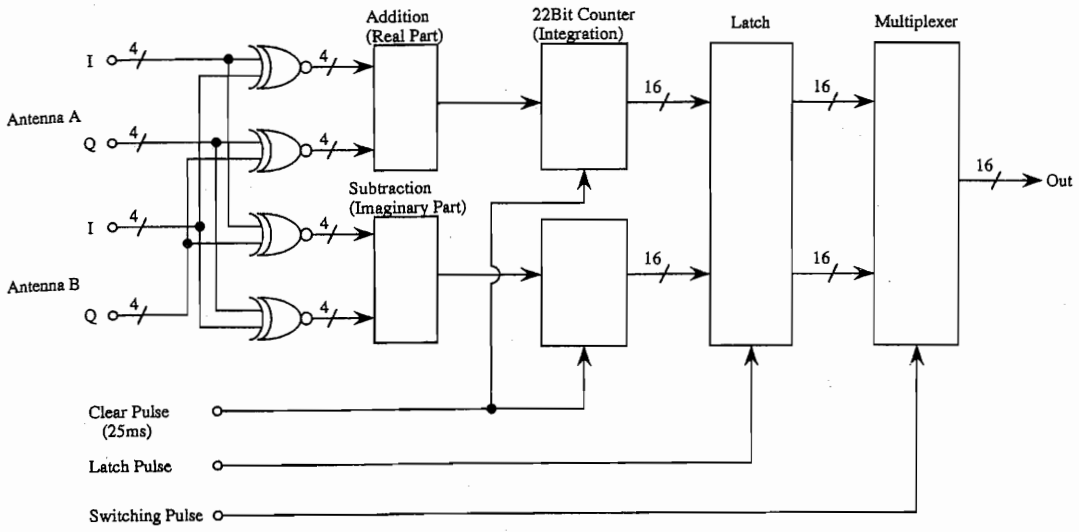

Fig. 6. An elementary circuit of the complex correlation LSI.

unit consists of four 4-bit- parallel exclusive-OR circuits, an addition and subtraction circuit, two integration circuits, a latch, and of a multiplexer circuit. The complex correlations for 3486 antenna pairs are measured by using 231 chips. Figure 8 shows a unit of the correlator chip. As the conventional clock rate of the CMOS gate array is 10 MHz and is one-quarter of the sampling clock at the A/D converter, the calculation in the correlator chip is performed in parallel by four sets of circuit after re-sampling the 40-MHz bit stream to four 10-MHz bit streams shifted by 25-ns interval of each other. The interval of data integration in the correlator chip is synchronized to the timing of the polarization switching of 25 ms. The integration time is 24.615 ms and the remaining 0.385 ms is a dead time to the transient of polarization switching.

The one-bit correlations result in the loss of amplitude information of measured Fourier components. Therefore, the signal strength, including the received signal and the receiver noise, is measured to each antenna using the square law detectors every 25 ms. The correlation data, together with amplitude data, are read out every 25 ms alternately for right- and left-handed circular polarization components, and are stored into buffer memories after the Van Vleck correction (Van Vleck and Middleton 1966) is applied. As a result, a complete set of complex correlation data is produced every 50 ms.

All data with 50-ms time resolution (50-ms data) are averaged for 1 s, and are stored in optical disks of 5 Gbytes after being sent to the host computer (NEC SX-JL). On the other hand, all original 50-ms data are recorded once every day in a high-density MT of 20 Gbytes using a high-speed digital data recorder (SONY DIR1000). After the end of daily observations, flares which occurred during the observation are searched with some criterion (such as flux density is greater than a pre-determined threshold), and the 50-ms data of the flares are played back and transferred to the host computer. These flare data are also saved on the optical disks of the host computer.

5. Fiber Optic Signal Transmission Lines

Fiber-optic signal transmission lines are extensively used in the radioheliograph. The optical fiber is especially suitable for cabling in small antennas. Single-mode optical fibers are used to transmit the IF signal from the front-end boxes to the observation building and the

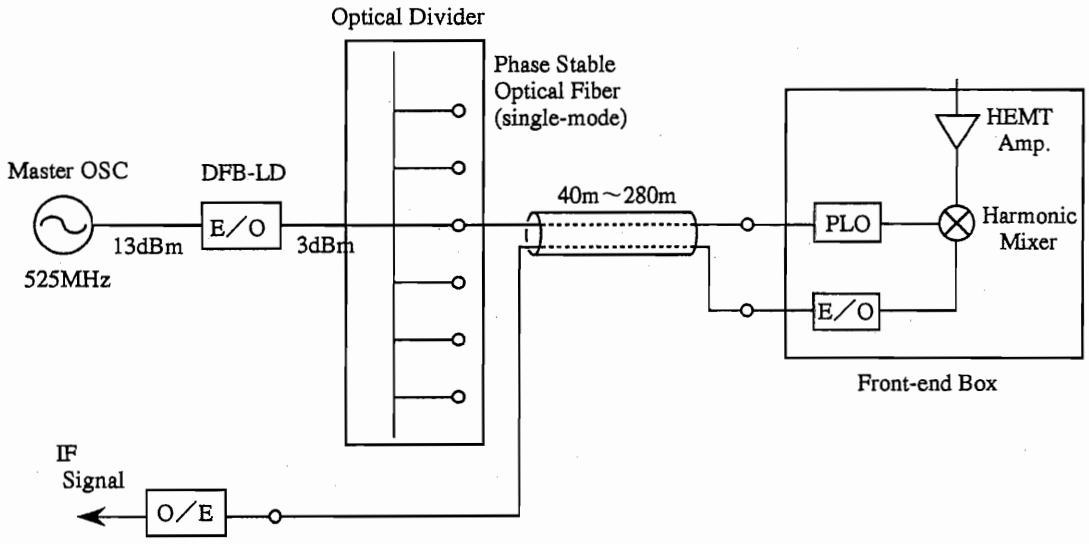

Fig. 7. Block diagram of the phase-lock network.

local reference signal from the observation building to the front-end boxes.

The optical fiber has advantages in that the transmission loss is very low and the bandwidth of the carrying RF signal is wide; therefore, the equalization of band characteristics for transmitted RF signals is not necessary, which is usually indispensable in case of coaxial cables. Optical fibers have also an advantage of producing no electrical interference. However, fiber-optic signal transmission lines have a disadvantage in that the dynamic range of the transmitted signal is limited because of poor S/N ratio as compared with coaxial cables. Further, they have limited maximum amplitude when electrical-to-optical converters (E/O converters) and optical-to- electrical converters (O/E converters) are used for analog signal transmission, as in the present case. This is especially severe in case of transmission of the IF signal, because the input signal of the E/O converter varies over a range of 21 dB, which corresponds to the ratio of the system temperature (910 K average) and the expected maximum antenna temperature from the Sun during radio bursts (10^5 K). The available dynamic range of the fiber-optic lines is only 16 dB in the present case, when the lowest signal level is kept 15 dB above the noise level of the O/E converter to avoid deterioration of the system S/N ratio. Actually, the dynamic range of the input signal to the E/O converters is limited to 11 dB by inserting 10-dB attenuation switches in the IF lines of the front-end receiver.

A phase-lock network using optical fibers are newly developed for the radioheliograph. This system is suitable for the connected array with large number of remotely placed antennas because of low signal transmission loss and simple structure. A block diagram of the phase-lock network is shown in figure 9. As the network is an open-loop type, temperature responses of the optical fiber cables govern the phase stability of the receivers. We are using a phase-stable optical fiber cable developed by Sumitomo Electric Industries Ltd (Tanaka et al. 1990). This cable has a temperature coefficient of 0.2 ppm/°C for temperature ranges from −10 °C to 20 °C. The cables are buried 1.2 m under the ground, where the temperature ranges from 4 °C to 10 °C and its variation is less than 0.1 °C/day and 10 °C/year. Accordingly, the phase stability of the 17-GHz signal due to temperature variations through the buried optical fibers is kept less than 0.°8 /day for a cable length of 280 m, which is the maximum difference among the receiver channels.

The internal noise caused by the fiber-optic devices reduces the C/N ratio of the 8.4-GHz local signal and degrades the level of correlation. The C/N ratio of the 525-MHz reference signal to 10-kHz offset point is about 110 dB/Hz, which is sufficient to produce clean local signals at 8.4 GHz, and thus the degradation of the correlation is less than 0.1 % (Nishio et al. 1992b).

In the radioheliograph, multi-mode optical fibers are also used to transmit timing pulses for polarization switches, 180 ° phase switches, and control signals of the 10-dB attenuation switches from the observation building to the front-end boxes.

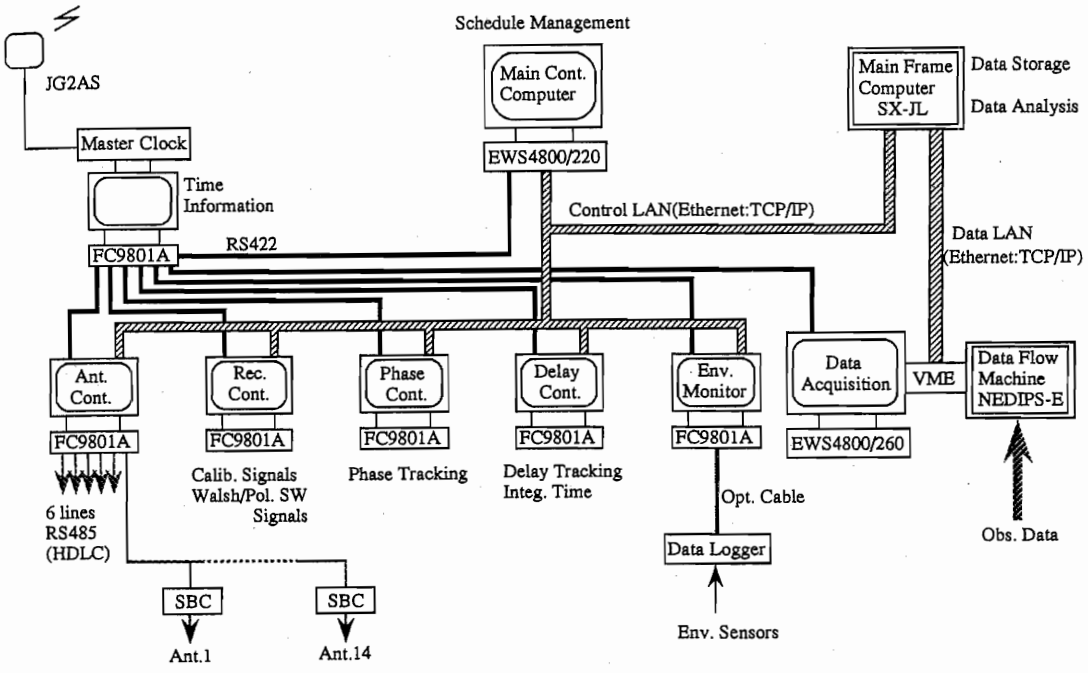

Fig. 8. Block diagram of the control system.

6. Control System

The control system of the radioheliograph is composed of three major logical components. Single-board computers (SBC) equipped with a 16-bit microprocessor are installed in each antenna, which provide the interface to the antenna hardware and the front-end receiver to be controlled or monitored. The intermediate level software running on five microcomputers (NEC FC9801A) in the observation building handles all the basic level microcomputers belonging to each antenna and the interface to the IF receiver and the digital back-end receiver. The high level software which performs the overall control is running on a workstation (NEC EWS4800/220) installed in the observation building. A block diagram of the control system is shown in figure 8. The SBCs installed in each antenna and one of the FC9801s are connected by twist-wire communication lines of the HDLC protocol. The PC9801s and the EWS4800 are connected by an Ethernet link. Fundamental control interval of the radioheliograph is 5 s. A pulse signal of 5-s interval generated at a master clock of the radioheliograph is distributed to all control components in order to synchronize the control timing to the master clock.

The SBCs control the stepping motors which drive azimuth and elevation axes of antennas. The FC9801 calculates the position of the Sun at every 5 s and sends them to the SBCs. Speed and direction of the stepping motors during next 5 s are calculated at the SBCs. The pulse signal with 5-s interval is distributed to the SBCs by twist-wire lines, and control processes required strict time synchronization are performed by the SBCs. Overall pointing accuracy of the antennas is better than $\pm$ 1.'5, which includes the mechanical pointing error and the error caused by the control algorithm. The SBCs also control switches in the front-end receivers which are used in the calibration mode of the radioheliograph. The SBCs monitor temperature of the front-end boxes, and condition flags of phase- locked oscillators and antenna position sensors.

Three of other four FC9801s are shared to control a phase tracking hardware, a delay tracking hardware, and switches for calibrations installed in the IF receiver, respectively. In the phase tracking and the delay tracking, hard-wired logic circuits perform processes required strict time synchronization, and the FC9801s share functions to calculate the tracking parameters and send them to the hard-wired logic circuits within 5 s. The remaining one of FC9801s is connected to environment sensors placed at antenna site, which monitor ambient temperature, humidity, wind speed and so on. These data are closely related with the phase fluctuations occurred in the earth atmosphere.

Routine observations are automatically performed according to a schedule table installed in the EWS4800. Basic parameters for the position of the Sun are stored in the EWS4800, and is broadcasted to the FC9801s before the start of observations. It is possible to change the observation schedule by modifying the schedule table or manually typing commands to the EWS4800. Overall man- machine interface to the radioheliograph is provided with the EWS4800, and usually a single operator can manage the observation. Basic-level man- machine interface to the radioheliograph is also provided by the FC9801s. When the malfunction occurred in the EWS4800 or the Ethernet link, control of the radioheliograph can be executed by setting the parameters and the commands to the FC9801s manually. There is no logical coupling among the SBCs. Therefore, even if some antennas get into troubles, observations can be continued by logically disconnecting the troubled antennas from the control system.

7. Total Performance

Image quality of the radioheliograph is largely influenced by correlator- based (baseline-based) amplitude and phase errors, which are given as a function of antenna combinations and cannot be removed by a self- calibration method using the redundant antenna combinations (Hanaoka et al. 1994b). In the radioheliograph, these errors are caused by unequal bandpass characteristics, antenna pointing errors, delay errors, and noise at correlator outputs. We evaluated the correlator-based errors using the closure relations, which give equivalent estimates of the correlator-based errors. Fluctuations of closure phase and amplitude were estimated for antenna combinations with short antenna spacing, and were within $\pm$ 0.°5 and $\pm$ 4%, respectively (Koshiishi et al. 1994). These values insure that the radioheliograph have a potential to produce images with dynamic range of 30 dB. However, the dynamic range of actual images is about 25 dB. This discrepancy is not caused by the radioheliograph's hardware, but by a limit of current image processing procedure.

From the start of routine observations on late June, 1992, the radioheliograph continues daily observations with very few days of data lack. We realize this by dual data recording system of the data storage computer and a high speed digital data recorder connected to the back-end receiver with hard-wired circuits, as well as the good stability of the radioheliograph's hardware. In addition, the fully distributed control system enables us operate the radioheliograph in conditions where some portions malfunction.

Acknowledgments

The authors are grateful to M. Ishiguro and K.-I. Morita of NRO for their valuable discussions in the design phase; and to Faculty of Agriculture, Shinshu University, for allowing us to use the radioheliograph antenna site. We also deeply acknowledge to many persons who supported this project. The Radioheliograph was supported by the Ministry of Education and Culture, Japan.

References

1. Baars, J. W. M. et al., 1973, *Proc. IEEE* **61**, 1258.
2. Enome, S. et al., 1993, *Proc. IAU Col.* **141**, 310.
3. Enome, S. et al., 1994, *Publ. Astron. Soc. Japan* **46**, L27.
4. Hanaoka, Y. et al., 1994a, *Publ. Astron. Soc. Japan* **46**, 205.
5. Hanaoka, Y. et al., 1994b, *in this proceedings.*
6. Koshiishi, H. et al., 1994, *Publ. Astron. Soc. Japan* **46**, L33.
7. Mishima, K. et al., 1992, *Japanese Assoc. of Surveyors, Tech. Rep.* (in Japanese).
8. Napier, P. J. et al., 1983, *Proc. IEEE* **71-11**, 1295.
9. Nakajima, H. et al, 1994, *Proc. IEEE* **82**, 705.
10. Nishio, M. et al., 1992a, *Proc. of IGARSS '92* **2**, 1435.
11. Nishio, M. et al., 1992b, *Proc. of ICALEPCS, KEK Proc.* **92-15**, 371.
12. Nishio, M. et al., 1994, *Publ. Astron. Soc. Japan* **46**, L11.
13. Shibasaki, K. et al., 1994a, *Publ. Astron. Soc. Japan* **46**, L17.
14. Shibasaki, K. et al., 1994b, *Space Science Review, submitted.*
15. Takakura, T. et al., 1994, *Publ. Astron. Soc. Japan, submitted.*
16. Takano, T. et al., 1994a, *Publ. Astron. Soc. Japan* **46**, L21.
17. Takano, T. et al., 1994b, *in this proceedings.*
18. Tanaka, S. at al., 1990, *KEK Report* **90-9**, 1.
19. Van Vleck J. H. and Middleton, D., 1966, *Proc. IEEE* **54**, 2.
20. Weinreb, S., 1963, *Research Lab of Electronics, MIT, Cambridge, MA, Tech. Rep.* **412**.

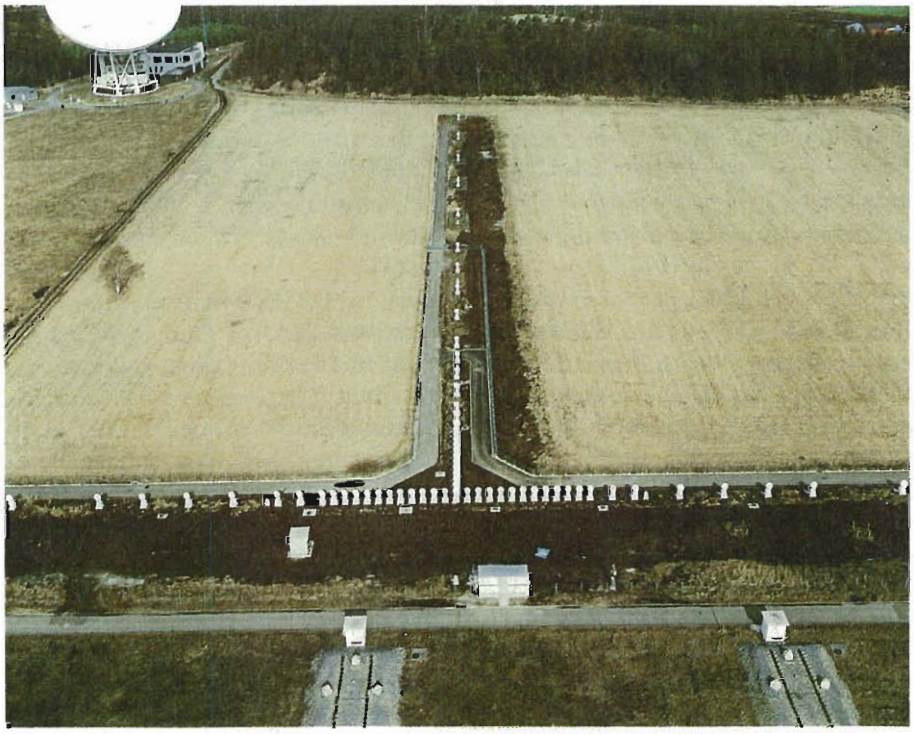

Photo.1. A view of the antenna array of the Nobeyama Radioheliograph.

Photo 2. A close-up of an element antenna.

Photo 3. A view of the IF receiver and the digital back-end receiver.